HERON contains contributions based mainly on research work performed in I.B.B.C. and STEVIN and related to strength of materials and structures and materials science.

Jointly edited by:

STEVIN-LABORATORY
of the Department of
Civil Engineering of the
Technological University, Delft,
The Netherlands
and
I.B.B.C. INSTITUTE TNO
for Building Materials
and Building Structures,
Rijswijk (ZH), The Netherlands.

EDITORIAL STAFF:

F. K. Ligtenberg, *editor in chief*
M. Dragosavić
H. W. Loof
J. Strating
J. G. Wiebenga

Secretariat:

L. van Zetten
P.O. Box 49
Delft, The Netherlands

HERON vol. 18
1972
no. 3

Contents

MODEL RESEARCH ON A PRESTRESSED CONCRETE PRESSURE VESSEL FOR A NUCLEAR POWER STATION

Th. Monnier
P. J. H. Schnackers
(IBBC)

MODEL RESEARCH ON A PRESTRESSED CONCRETE PRESSURE VESSEL FOR A NUCLEAR POWER STATION

Summary

Research on a realistic prestressed concrete model of a pressure vessel for a gas-cooled nuclear reactor is described. The object of the research was to determine the nature of the failure and the ultimate load of such a structure under conditions similar to those in reality, i.e., with loading applied by internal gas pressure.

The model pressure vessel was in the shape of a (vertical) cylinder with flat end slabs and was made of prestressed micro-concrete. The prestress was produced by a system of straight and curved tendons, namely, 276 straight wires for the vertical prestress and 624 circular curved wires for the horizontal prestress (all wires 3 mm diameter, steel grade QP 160). The quantity of prestressing steel installed was based on a value of $\gamma = 3$ as is commonly adopted for the margin between working load conditions and failure for structures of this kind. The magnitude of the prestress was based on the criterion of cracking, i.e., under working load conditions the concrete stresses in the critical zones of the structure had to be zero. Conventional (untensioned) reinforcing steel was installed in addition to prestressing steel.

In this report the construction, the prestressing and the testing of the model are described in detail. The model was first subjected to internal oil pressure in the laboratory, the maximum pressure applied being 4.5 MPa (45 kg/cm^2). Next, the model was taken to a military explosives testing site, where it was tested by loading it by internal gas pressure. This pressure was slowly increased until explosive failure of the model occurred at an internal pressure of 12.9 MPa (129 kg/cm^2). The margin $\gamma = 3$ between working pressure and failure of the model was therefore duly attained. Despite the explosive character of the failure it was preceded by considerable deformations of the vessel after cracking had occurred. Hence this cannot be described as "sudden failure" in the normal sense of the term. The conclusion to be drawn from the tests is that the safety of prestressed concrete pressure vessels calls for closer attention than had originally been supposed.

Acknowledgment

The model testing on which is reported in this publication forms part of the total investigation which is being carried out on pressure vessels for nuclear power stations by the IBBC in co-operation with the Project Group Nuclear Energy. The above within the scope of the activities which the Project Group is carrying out in connection with power supply by means of nuclear power.

The investigation on the model of the prestressed concrete pressure vessel was carried out in the laboratory of the IBBC in 1970.

Many co-operators of the IBBC have given their appreciated co-operation in this investigation. The report originally written in the Dutch language, was translated by Ir. A. C. van Amerongen.

Samenvatting

Het onderzoek wordt beschreven, dat is uitgevoerd aan een realistisch voorgespannen betonmodel van een drukvat van een gasgekoelde kernreactor. Het doel van dit onderzoek was de aard van bezwijken, alsmede de uiterste belasting van een dergelijke constructie vast te stellen onder reële omstandigheden, d.w.z. bij belasten door inwendige gasdruk.

Het model-drukvat had de vorm van een (staande) cilinder met vlakke eindplaten en werd gemaakt van voorgespannen micro-beton. Het voorspansysteem bestond uit rechte draden voor de verticale voorspanning – 276 draden ∅ 3 mm, QP 160 – en uit cirkelvormig gebogen draden voor de horizontale voorspanning – 624 draden ∅ 3 mm, QP 160. De hoeveelheid voorspanwapening is gebaseerd op een, voor dergelijke constructies gebruikelijke, marge $\gamma = 3$ tussen gebruiks- en bezwijktoestand, terwijl de grootte van de voorspanning werd afgestemd op het criterium, waarbij onder bedrijfsomstandigheden geen betontrekspanningen optreden. Naast de voorspanwapening werd tevens betonstaalwapening aangebracht.

In dit rapport worden de bouw, het voorspannen, alsmede de beproeving van het model uitvoerig beschreven. Het model werd eerst in het laboratorium belast d.m.v. oliedruk. De maximum druk bedroeg hierbij 4,5 MPa (45 kgf/cm²). Aansluitend werd het model getransporteerd naar een militair springterrein, waar het werd belast door middel van gasdruk. Deze gasdruk werd langzaam verhoogd tot het model explosief bezweek bij een inwendige druk van 12,9 MPa (129 kgf/cm²). De marge $\gamma = 3$ t.o.v. de bedrijfsdruk m.b.t. bezwijken van het model werd dus inderdaad bereikt. Ondanks het explosieve karakter van het bezwijken traden vóórdien in het vat nog grote vervormingen op na scheurvorming. Er kan dus niet worden gesproken van plotseling bezwijken in de normale zin. De conclusie is, dat de veiligheid van voorgespannen betondrukvaten toch meer aandacht verdient, dan men aanvankelijk eraan dacht te moeten besteden.

SI-units

The units applied in this article have been taken from the international system of units (SI-Système International d'unités).
The basic units for length and mass are 1 m (meter) and 1 kg (kilogram) resp. The derived unit for force is 1 N (Newton).
Recently as SI-unit for stress 1 Pa (Pascal) has been accepted, in which 1 Pa = 1 N/m^2. Thereby prefixes must be used which are cube numbers of 10, like M (mega) = 10^6, G (giga) = 10^9, μ (micro) = 10^{-6} and p (pico) = 10^{-12}, besides the already known indications as k (kilo) = 10^3 and m (milli) = 10^{-3}.
For the sake of "recognition" forces have also been indicated in kg (kilogram) and lengths in cm (centimeter). Thereby it has been accepted that 1 N = 0.1 kg, so that 1 MPa = 10 kg/cm^2, 1 kN = 100 kg and 1 kNm = 100 kgm.

Nuclear power station in principle

In principle a nuclear power station works as follows:
Fission of radioactive materials takes place in the so-called core of the reactor. The fission fragments release kinetic energy which is given off to the surroundings in the form of heat. In order to utilise this heat it is necessary to let the fission process take place in a suitable medium – the primary coolant – which may, for example, be a gas. The primary coolant is circulated by pumping it through heat exchangers in which the heat which it conveys is transferred to water circulating in a separate second circuit. This water – the secondary coolant – is used for generating steam which in turn is used for driving electricity generating plant in much the same way as is done in a thermal (conventional) power station. The conditions as to pressure, temperature and radioactivity in the primary circuit differ according to the type of nuclear reactor, the heat transfer medium employed, from the conditions in the steam generating circuit. The latter is free from radioactivity.

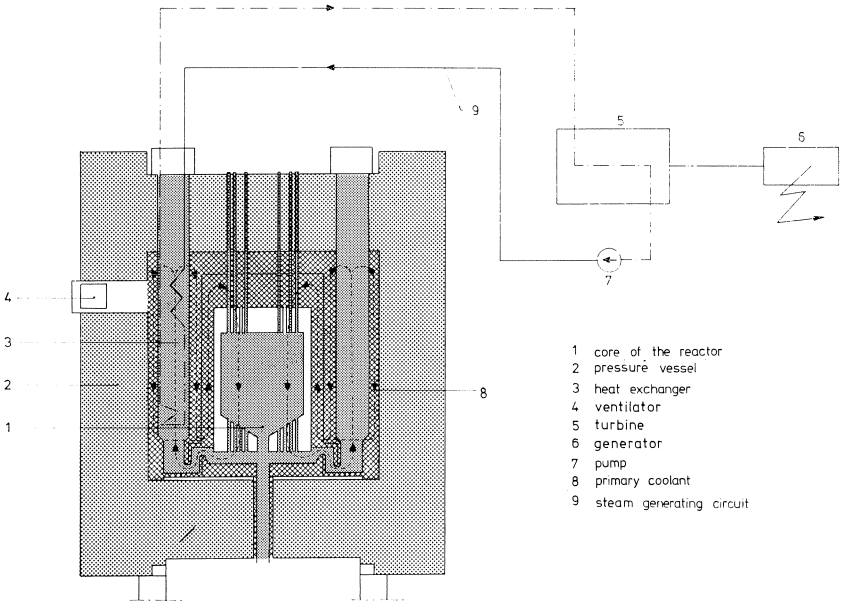

Model research on a prestressed concrete pressure vessel for a nuclear power station

(gas-cooled reactor)

1 Introduction

In recent years there has been a marked increase in the interest focused on prestressed concrete pressure vessels. This has been due mainly to the increase in the dimensions of the pressure vessels for nuclear power stations. Considerations of economy as well as safety play a part in this context:

- with larger power stations, which of course require larger pressure vessels but obviously also have a higher generating capacity, electric energy can be produced relatively more cheaply;
- for reasons of safety it is the aim of designers to enclose the whole primary circuit of gas-cooling within the pressure vessel.

In the smaller nuclear power stations a steel pressure vessel functions as a structural component and withstands the high internal pressure around the reactor. In that case, however, it is necessary to surround the pressure vessel by a biological shield, constructed of concrete, as a safeguard against radioactive radiation. Because of the larger dimensions now required for pressure vessels, it has become increasingly attractive to use prestressed concrete for their construction. Such pressure vessels have the added advantage that they themselves can serve also to provide biological shielding.

2 Object of the research

In connection with the construction of the larger nuclear power stations the responsible authorities have hitherto always insisted that a model (scale 1:5 to 1:10) of the prestressed concrete pressure vessel be made, with the object of testing its behaviour under service conditions and determining the margin with regard to failure, the results of such tests thus providing verification of the design calculations.

In such tests the internal pressure in the model was always applied by hydraulic means, i.e., with water or oil. Under these circumstances the excess pressure quickly diminishes in consequence of leakage of the liquid through cracks extending all the way through the structure. When the pressure thus drops, the cracks close up again. From this behaviour it was at first inferred that the vessels under consideration could not possibly develop failure of an explosive character.*)

---

*) See "Discussion", Group B: "Design Philosophy. Criteria and Safety." Conference on prestressed concrete pressure vessels, Westminster, London, S.W.1, 13-17 March, 1967.

The research described here relates to a realistic concrete model which was loaded to failure by internal gas pressure.

This method of loading the pressure vessel is in closer conformity with reality than loading by hydraulic pressure and involves a much higher energy input into the vessel. The object of the research was to determine the nature of failure, the failure mechanism and the ultimate load under these realistic conditions.

3 The model

The model under consideration was in the shape of a (vertical) cylinder with a bottom slab and a cover slab at its ends. This shape has, so far, almost invariably been adopted for prestressed concrete pressure vessels because it enables a reasonable compromise to be effected between a practicable method of prestressing and a favourable pattern of action of the forces.

The dimensions of the model pressure vessel were based on data obtained from the literature [1–5]; they are indicated in Figs. 1, 2 and 3. The model was made of microconcrete. The prestress was applied in accordance with the system described in [3]. This comprises a vertical prestress produced by vertical wires and a horizontal prestress produced by circular curved wires as shown in Figs. 2 and 3, in which the location of the vertical prestressing wires is also indicated. The successive layers of horizontal annular tendons were positioned in relation to one another in the manner shown in Fig. 4. Two successive layers together produce a complete circumferential prestress. The projections on the external surface of the cylinder were needed for anchoring the horizontal tendons.

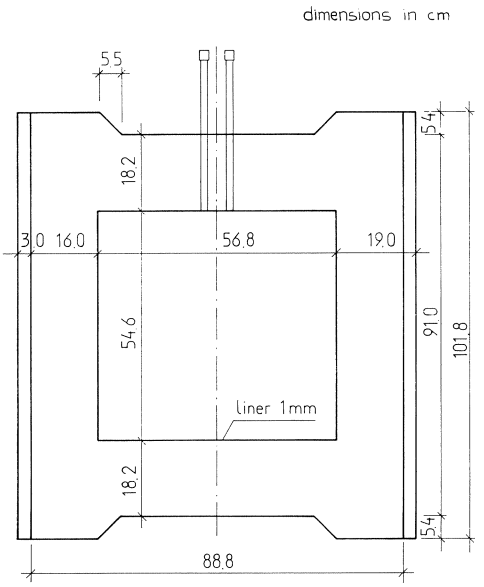

Fig. 1.
Vertical section through pressure vessel: dimensions, shape.

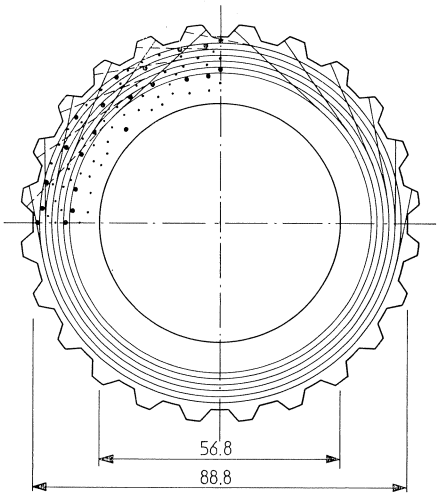

Fig. 2.
Horizontal section through cylindrical wall of pressure vessel: prestressing steel.

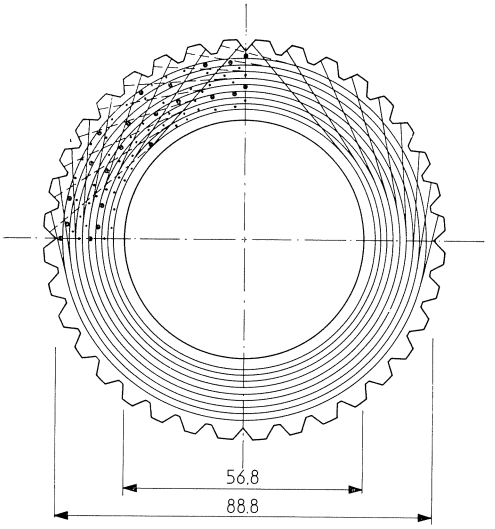

Fig. 3.
Horizontal section through pressure vessel at bottom or top slab: prestressing steel.

Fig. 4. Location of horizontal tendon layers in relation to one another.

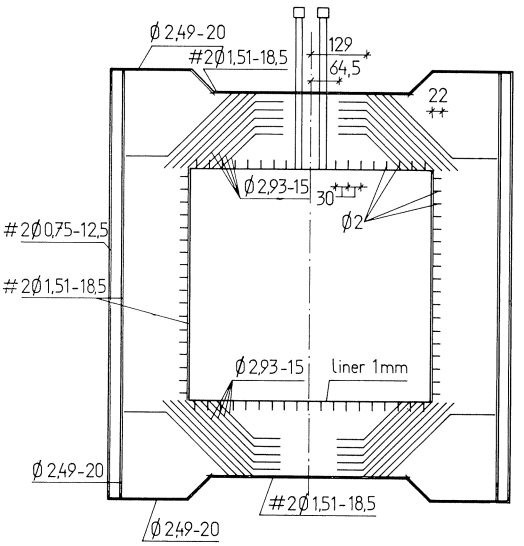

Fig. 5.
Vertical section through pressure vessel: untensioned reinforcing steel.

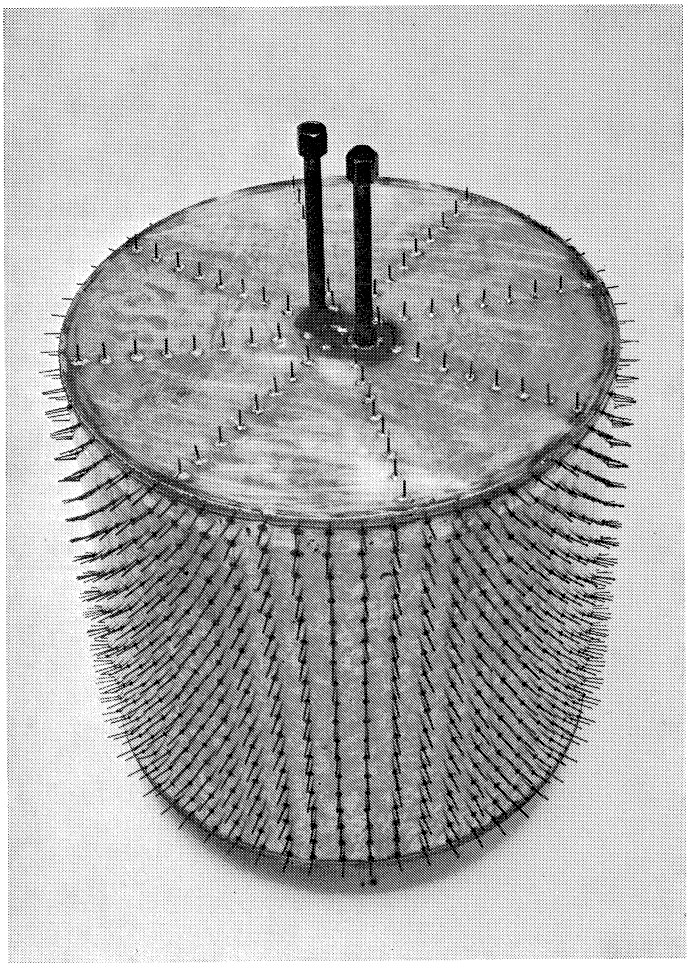

Fig. 6.
The liner

In addition to prestressing steel the model also contained untensioned steel reinforcement (see Fig. 5). The steel liner in the pressure vessel was likewise provided – suitably reduced to scale – in the model and was provided with the necessary anchorages (see Fig. 6).

4 Simplifications

As already stated, the object of the research was to obtain accurate information on the failure of the model pressure vessel. This made it necessary to construct the model as realistically as possible with regard to its shape, prestressing system and steel liner. As interest was focused on the overall behaviour of the vessel, the various apertures through the wall, which are present in an actual pressure vessel, were entirely omitted in the model, though of course a connection to the exterior had to be provided to enable the model to be loaded by internal pressure.

Testing was carried out as simply as possible. Elevated temperature was unnecessary within the context of this research, and the test was accordingly performed at normal ambient temperature.

Also, instrumentation was kept down to a minimum; only those measurements were carried out which enabled the overall deformation of the vessel, both in the vertical and in the circumferential direction, to be recorded at the various values of internal pressure.

5 Stresses in the model

With due regard to the loading conditions for the pressure vessels [1–5] of which the vessel under present consideration was a model, the working pressure adopted was 4 MPa (40 kg/cm^2). The stresses associated with this were calculated by elementary methods and are summarised in Table 1. The calculation is given in Appendix 1.

Table 1. Stresses in the (model) pressure vessel.

	calculated stresses in MPa						
	longitudinal direction σ_v			circumferential direction σ_h			
	internal surface	external surface	centre	internal surface	external surface	centre	
loading case	σ_{vi}	σ_{vu}	σ_{vm}	σ_{hi}	σ_{hu}	σ_{hm}	
in wall							
working pressure 4 MPa	+2.78	+2.78	+2.78	+9.55	+5.54	+7.10	
temperature gradient 20 °C	−5.40	+4.00	−0.09	−5.40	+4.00	+0.32	$\alpha_t=10^{-5}/°C$; $\nu=0.15$ and $E_b'=40$ GPa
working pressure + temperature gradient	−2.62	+6.78	+2.69	+4.15	+9.54	+7.42	
in cover and bottom							
working pressure 4MPa				+14.40	+7.62	+9.74	
temperature gradient 20°C				−5.40	+4.00	+0.32	(see above)
working pressure + temperature gradient				+9.00	+11.62	+10.06	
in wall							
prestress	−6.78	−6.78	−6.78	−16.46	− 9.54	−12.23	
in cover and bottom							
prestress				−21.95	−11.62	−14.84	

6 Prestressing reinforcement

The total requisite quantity of prestressing steel was determined from the average stresses calculated for the model subjected to the working pressure of 4 MPa

(40 kg/cm^2). It was decided to prestress the model with 3 mm diameter wires of steel grade QP 160. The stress-strain diagram for these wires is given in Fig. 7.

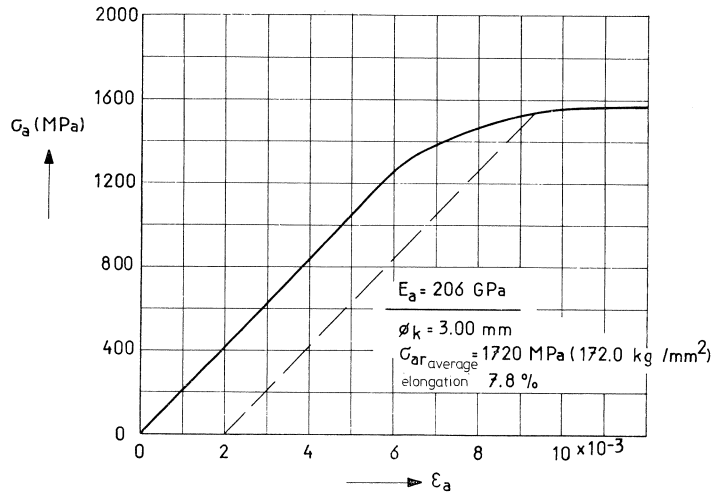

Fig. 7.
Stress-strain diagram of the prestressing steel: 3 mm diameter wires, grade QP 160.

It was also adopted as a condition that at 3 times the working pressure the prestressing steel alone must still just be able to resist the forces then occurring. This condition corresponds to the margin $\gamma = 3$ normally adopted for such pressure vessels. The minimum quantity of steel required is therefore:

a. Vertical prestressing steel:

$$\frac{3 \cdot 2.78 \cdot [\pi(568+888)/2] \cdot 160}{(\pi \cdot 3^2/4) \cdot 1600} = 276 \text{ wires 3 mm dia } (= 1948.56 \text{ mm}^2)$$

b. Horizontal prestressing steel:
- In the wall (assumed centre-to-centre spacing of the layers of prestressing steel 10.9 mm, two layers being needed to produce one complete annular prestress; see Figs. 8 and 4):

$$\frac{3 \cdot 7.10 \cdot 2 \cdot 10.9 \cdot 160}{(\pi \cdot 3^2/4) \cdot 1600} = 6 \text{ wires 3 mm dia per layer } (= 42.36 \text{ mm}^2)$$

- In the bottom slab and cover slab: on the assumption of a shearing plane at 60^c (see Appendix 1) the prestressing force which occurs here is found to correspond to an "internal pressure" equal to approximately 1.4 times the working pressure on the wall of the vessel. Accordingly, it is necessary to provide layers of prestressing steel comprising 9 wires of 3 mm diameter (= 63.54 mm^2) per layer, these layers being spaced at 10.4 mm centre-to-centre.

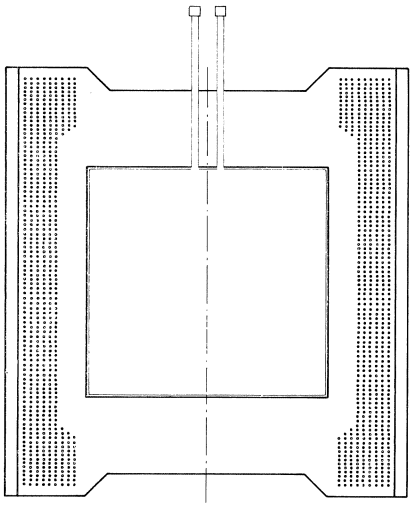

Fig. 8.
Vertical section through pressure vessel: horizontal prestressing steel.

Thus, in all, the horizontal prestressing steel consisted of 624 wires of 3 mm diameter (= 4405.44 mm^2).

7 Prestress

For determining the magnitude of the prestress to be applied it was assumed that the largest tensile stresses caused by the working pressure and the temperature gradient must be entirely cancelled by prestress. Hence under normal operating conditions the stress in the concrete at the points in question is 0 MPa; the safety against cracking would then have to be derived from the available tensile strength of the concrete.

The figures for the requisite prestress are summarised in Table 1, whence it follows that the magnitude of the prestress to be applied to the concrete must have the following average values:

a. In the vertical direction:
6.78 MPa (67.8 kg/cm^2), i.e., a steel stress of:

$$\frac{6.78 \cdot [2\pi(568+888) \cdot 160]/2}{1948.56} = 1270 \text{ MPa } (127 \text{ kg/mm}^2)$$

b. In the horizontal direction:
In the wall: $(9.54/5.54) \cdot 7.10 = 12.23$ MPa (122.3 kg/cm^2), i.e., per layer a prestressing force $= 12.23 \cdot 2 \cdot 10.9 \cdot 160 \cdot 10^{-3} = 42.60$ kN (4.26 t), and a steel stress $= 42.60 \cdot 10^3 / 42.36 \cdot 10^{-6} = 1010$ MPa (101 kg/mm^2).

In the bottom slab and cover slab:
$(11.62/7.62) \cdot 9.74 = 14.84$ MPa (148.4 kg/cm^2), i.e., per layer a prestressing force $= 14.84 \cdot 2 \cdot 10.4 \cdot 160 \cdot 10^{-3} = 49.40$ kN (4.94 t), and a steel stress $= 49.40 \cdot 10^3 / 63.54 \cdot 10^{-6} = 778$ MPa (77.8 kg/mm^2).

8 Frictional losses

As already stated, the prestressing system comprised straight wires for the vertical prestress and rather considerably curved wires for the horizontal prestress. Some of the vertical wires (80 of them) were installed in brass tubes (5 mm external, 4.5 mm internal diameter).

The average frictional loss for these wires was 15% (further particulars concerning frictional losses are given in Appendix 2). The initial prestressing force for the wires ($F_{\text{wires}} = 7.06$ mm^2), tensioned from one end, therefore had to be at least: $7.06 \cdot 1270/(1-0.15) = 10500$ N ~ 10 kN (1 t) in order to obtain sufficient prestress everywhere. The initial prestressing force P_A is the force which is applied to the ends of the tendons (wires) on first tensioning them. As a result of losses due to slip this initial force undergoes an average decrease of about 15% at the very outset. The maximum force in the wires is then about $0.90P_A$ on average (see Fig. 2.1, Appendix 2).

The other vertical wires were accommodated in 4.5 mm diameter ducts which had been pre-formed in the concrete with the aid of plastic-sheathed wire which was removed after the concrete had hardened. The prestressing steel subsequently inserted into these ducts was therefore in direct contact with the concrete. The frictional loss in this case was assumed to be equal to that occurring in the vertical prestressing wires installed in brass tubes.

The initial prestressing force adopted for all the vertical wires was 10 kN (1 t), corresponding to about 90% of the ultimate tensile fracturing force.

All the wires for producing the horizontal prestressing force were also installed in ducts (4.5 mm diameter) which had been pre-formed in the concrete with the aid of plastic-sheathed wire. For determining the initial prestressing force the frictional losses were of course also taken into account in order to ensure adequate prestress all round. For simultaneous tensioning of the wires at both ends the average frictional loss was found to be 33% (see Appendix 2).

The initial prestressing force to be applied therefore had to be at least:
$7.06 \cdot 1010/(1-0.33) = 10650$ N ~ 10 kN (1 t).

Hence a value of 10 kN, corresponding to about 90% of the ultimate force, was adopted for the initial prestressing force in the horizontal wires, just as in the vertical wires. Here the initial prestressing force P_A is the tensioning force applied to both ends of each wire so as to retain sufficient prestress after deduction of the frictional losses. As a result of losses due to slip this force P_A is reduced at the outset, so that the maximum force in the wires is then $0.84P_A$ (= 8.4 kN) on average (see Fig. 2.2 and Fig. 2.3, Appendix 2).

9 Untensioned reinforcement

The (untensioned) reinforcing steel installed near the outer and inner surfaces of the wall was provided in order to distribute any cracking due to shrinkage of the concrete

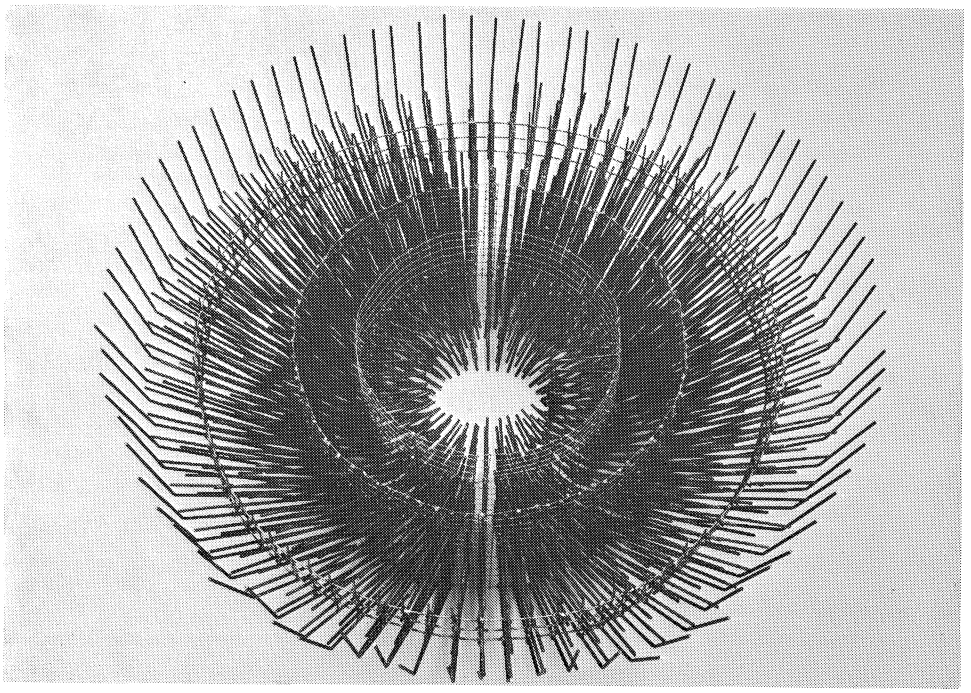

Fig. 9. Reinforcement cage for bottom slab or top slab.

and/or stress concentrations (see Fig. 5). The quantity of this reinforcement was determined with reference to information contained in [2]. Furthermore, reinforcement was installed in the projections on the exterior of the cylinder, these having been provided, as already stated, for anchoring the horizontal prestressing steel.

The reinforcement cages incorporated in the bottom slab and cover slab consisted of 2.93 mm diameter wires with a tensile strength of 553 MPa (5530 kg/cm^2) and served to prevent premature failure as a result of shear force (see Figs. 5 and 9). The quantity of reinforcing steel in these two slabs was so determined that at the failure stage the entire shear force could still just be resisted by this steel (see Appendix 1).

The concrete cover to the (untensioned) reinforcement at the outer and inner surface of the model was always 3 mm.

10 Properties of the micro-concrete

The micro-concrete used for making the model was composed as indicated in Table 2.

For the sake of good workability of the concrete for a relatively long time, high-alumina cement was used. This type of cement has the additional advantage that the concrete reaches its eventual strength at an age of only 7 days. In this way it was possible to minimise the effect of having to concrete the pressure vessel in two stages, as was unavoidable (see Section 11).

Table 2. Particulars of the micro-concrete used for the model:
cement/aggregate ratio (dry) = 0.25 (parts by weight);
type of cement: high-alumina;
water/cement ratio = 0.55;
aggregates: fineness modulus = 2.97; maximum particle size 2.8 mm.

concreting	stage I					stage II		
tested after n days	1	7	14	17	44	3	6	33
strength values								
compressive (cube) strength (7.1 cm · 7.1 cm · 7.1 cm) MPa	49.3	62.1	67.4	67.5	67.5	49.6	56.4	61.9
prism strength (10 cm · 10 cm · 30 cm) MPa						34.3		38.4
flexural strength (10 cm · 10 cm · 30 cm) MPa								4.09
splitting tensile strength (7.1 cm · 7.1 cm · 7.1 cm) MPa				4.02	4.61		3.81	4.29
splitting tensile strength (10 cm · 10 cm · 15 cm) MPa								3.56
modulus of elasticity (10 cm . 10 cm · 30 cm) GPa							33.5	32.3
bulk density (10^3 kg/m^3)	2.30	2.31	2.30	2.29	2.30	2.30	2.30	2.28

The strength figures for the concrete employed are also given in Table 2. They were determined on 7.1 cm cubes and on 10 cm · 10 cm · 30 cm prisms. The average stress-strain diagram for the concrete is presented in Fig. 10, while in Fig. 11 the shrinkage has been plotted as a function of time.

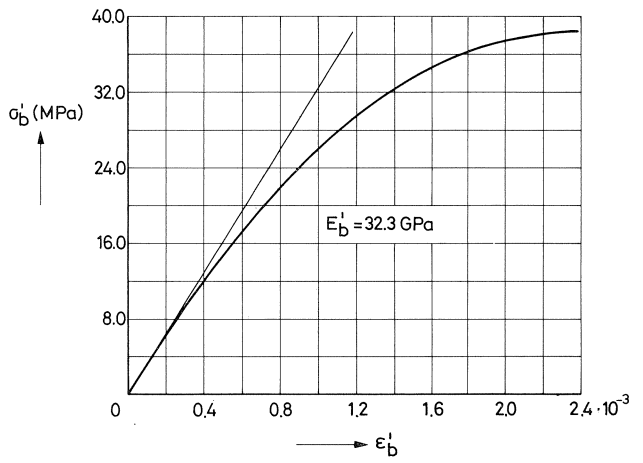

Fig. 10.
Average stress-strain diagram of the concrete at an age of 33 days.

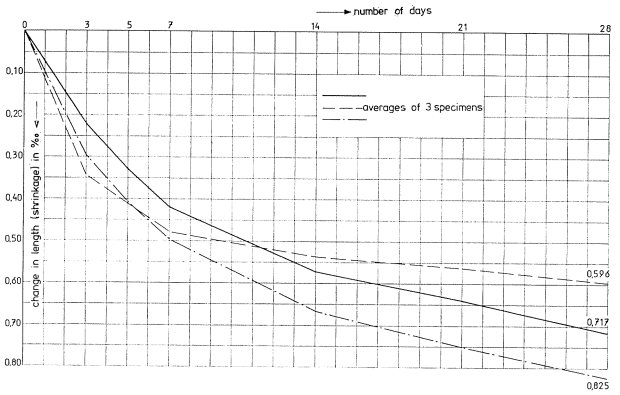

Fig. 11. Change in length (in $^0/_{00}$) of three series of concrete prisms (4 cm · 4 cm · 16 cm) at 20 °C and 65% relative humidity.

11 Construction of the model

Before construction of the model was commenced, the following components were prefabricated: the liner (Fig. 6), the fixing rings for assembling the horizontal prestressing tendons (Fig. 12), the (untensioned) steel reinforcement, the reinforcement cages for the bottom slab and cover slab (Fig. 9), and the formwork (in five parts). These components were assembled in accordance with the detailed scheme given in Appendix 3 (see Figs. 13–16).

The model had to be concreted in two stages. The construction joint was located about 5 cm below the top of the liner; the latter served as internal formwork for the wall of the cylinder. One day after completion of concreting all the plastic-sheathed wires (and all the plastic sheathing) were withdrawn from the concrete (see Fig. 17). The prestressing steel was then inserted into the ducts thus formed. Finally, the pressure vessel was prestressed. The tendons were not grouted. Fig. 18 shows the model after prestressing had been carried out.

Further information on the concreting and tensioning operations is given in Appendix 3.

12 Test-procedure

Testing the model was done in two stages: stage I with oil pressure, stage II with gas pressure (nitrogen). In stage I the oil pressure was applied in incremental steps of 0.5 MPa (5kg/cm^2), up to a maximum of 4.5 MPa (45kg/cm^2). At each step in the load application procedure the horizontal and vertical deformations were measured by means of displacement transducers (Fig. 19). The results of these measurements are presented in Fig. 25.

Fig. 12.
Forming ring for the horizontal prestressing steel in bottom slab or cover slab.

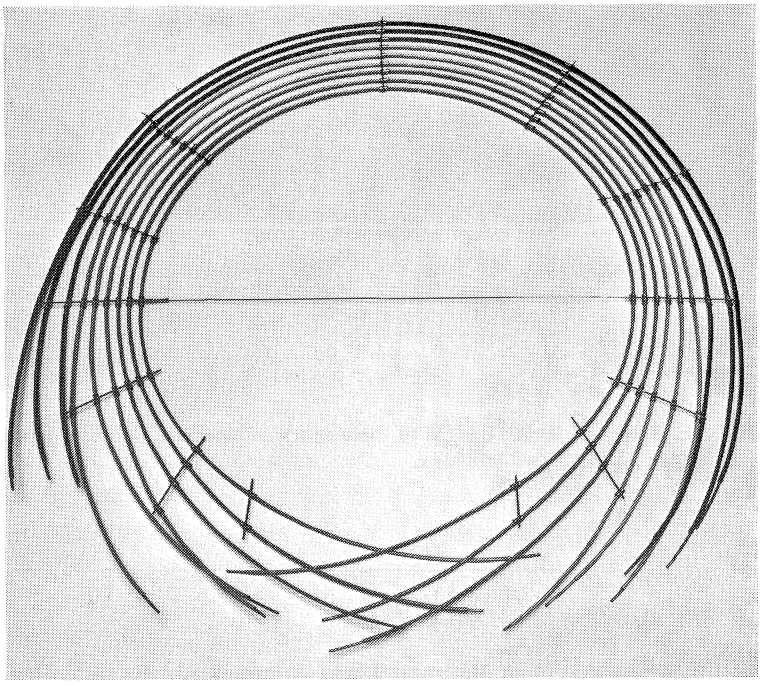

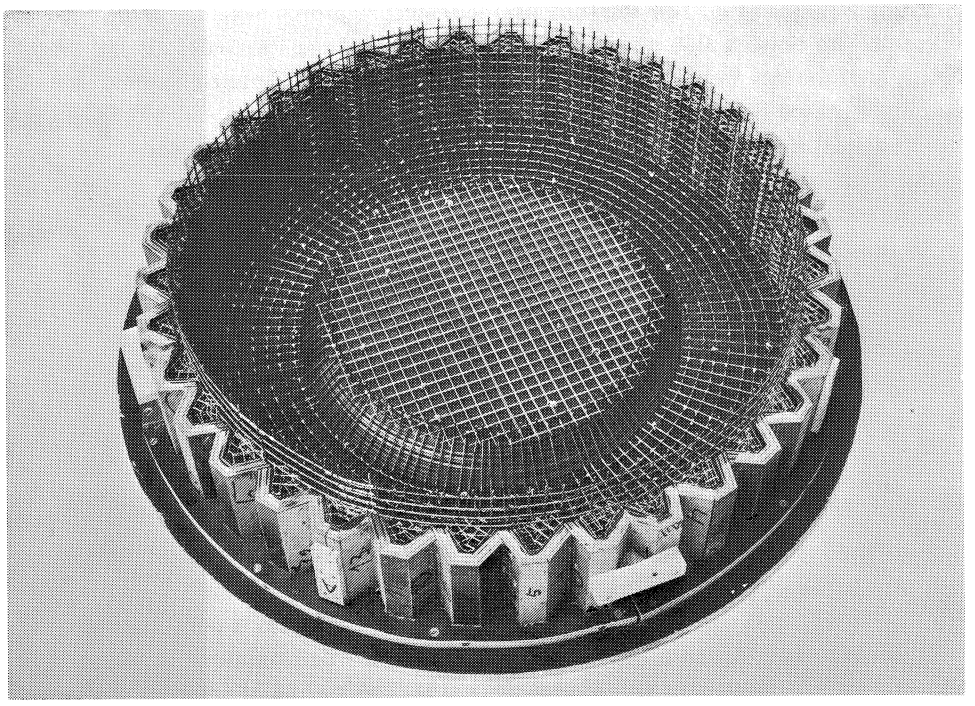

Fig. 13. Formwork with reinforcement for bottom slab.

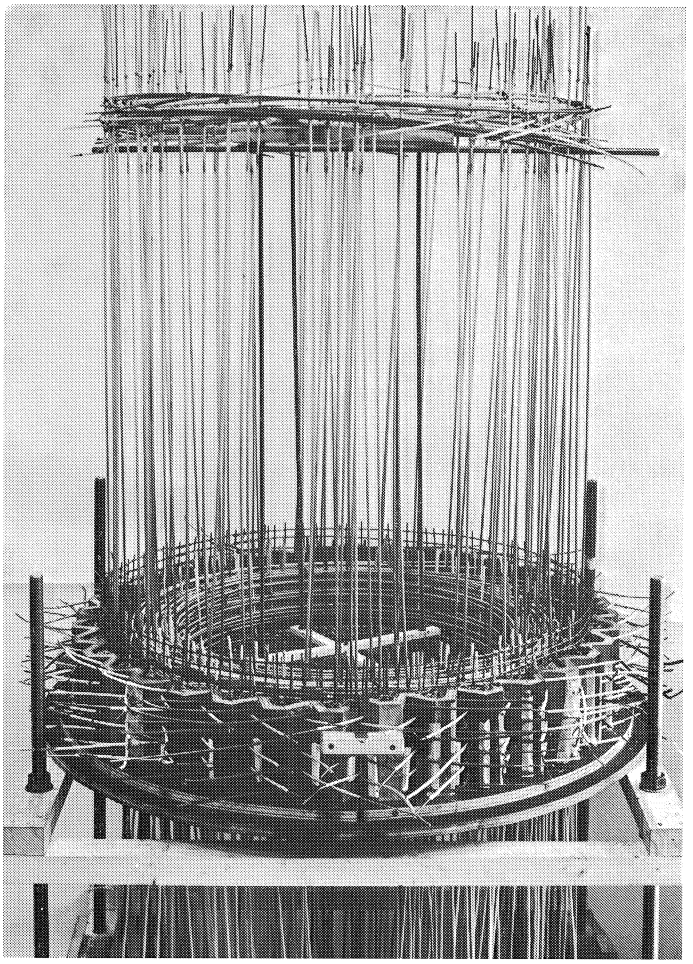

Fig. 14 Assembly in preparation for concreting: forming rings for horizontal prestressing steel in bottom slab have been installed.

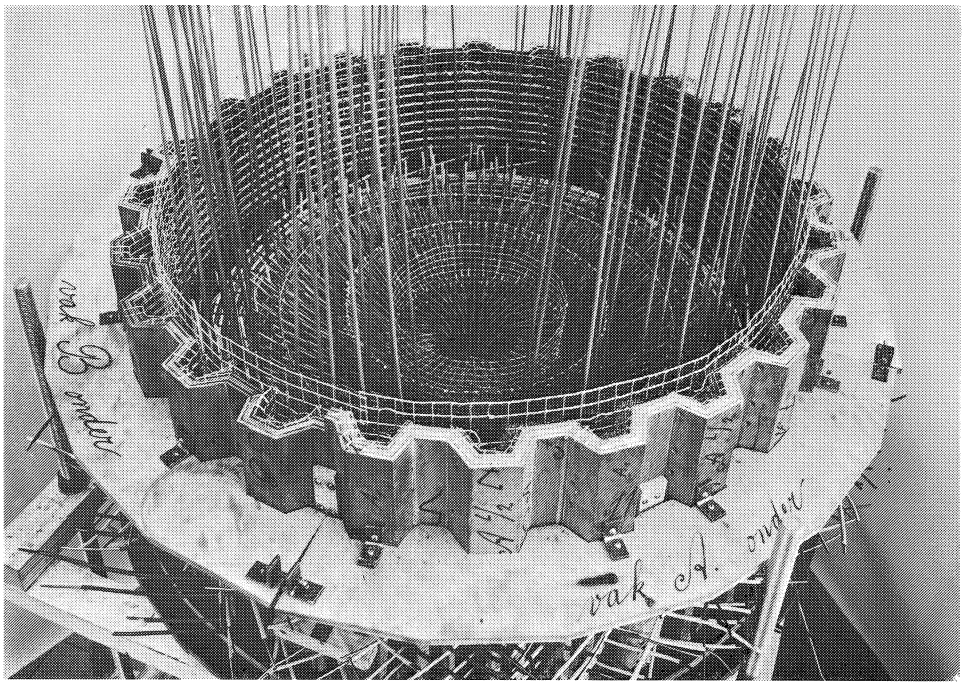

Fig. 15a.

Fig. 15b.

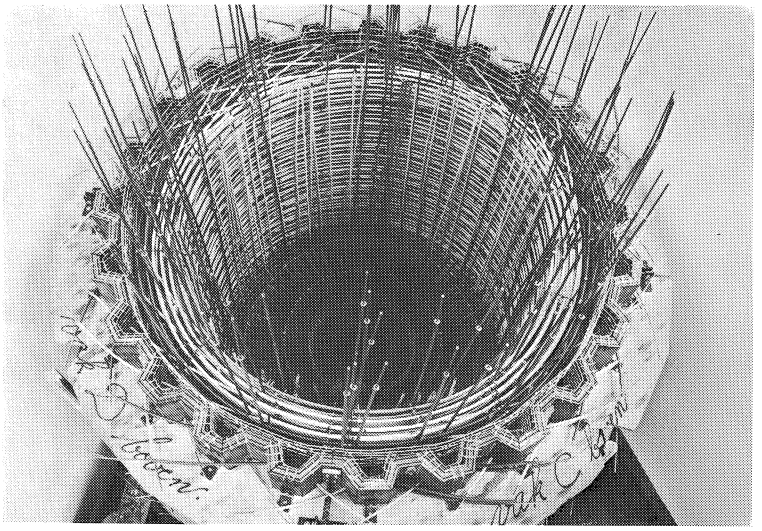

Fig. 15. Assembly in preparation for concreting: reinforcement cage for bottom slab has been installed.

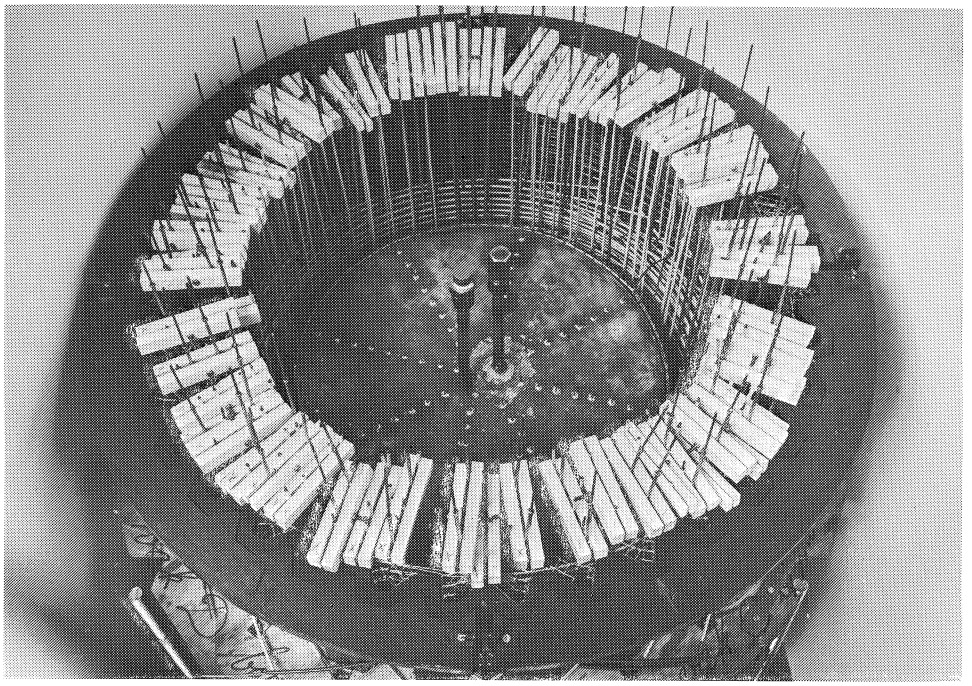

Fig. 16. Assembly in preparation for concreting: liner has been installed.

For reasons of safety, loading the model with internal gas pressure (stage II) was done on a site used for the testing of military explosives. After each load application step the deformations were measured again. Fig. 20 shows the model just before loading was commenced. The connection for applying the gas pressure and the auxiliary structure supporting the displacement transducers are also seen in this photograph (see also Fig. 19).

The operations of increasing the gas pressure and of measuring and recording the deformations were controlled from a nearby bunker. Two television cameras and a cine camera were installed in the vicinity of the pressure vessel. The equipment in the bunker included a television receiver and a video recorder to enable the behaviour of the model under load to be visually examined as well as recorded.

Failure of the model occurred at an internal pressure of 12.9 MPa (129 kg/cm^2) and was marked by a violent explosion. The upper part was torn off the bottom slab and ended up at a distance of about 3 m from its original position. It is estimated that this part of the vessel was thrown about 10 m into the air (see Fig. 21: 6 images per 5 seconds). Fig. 22 shows the model after testing. The cracking that occurred in the wall and in the cover slab of the model is illustrated in Figs. 23 and 24.

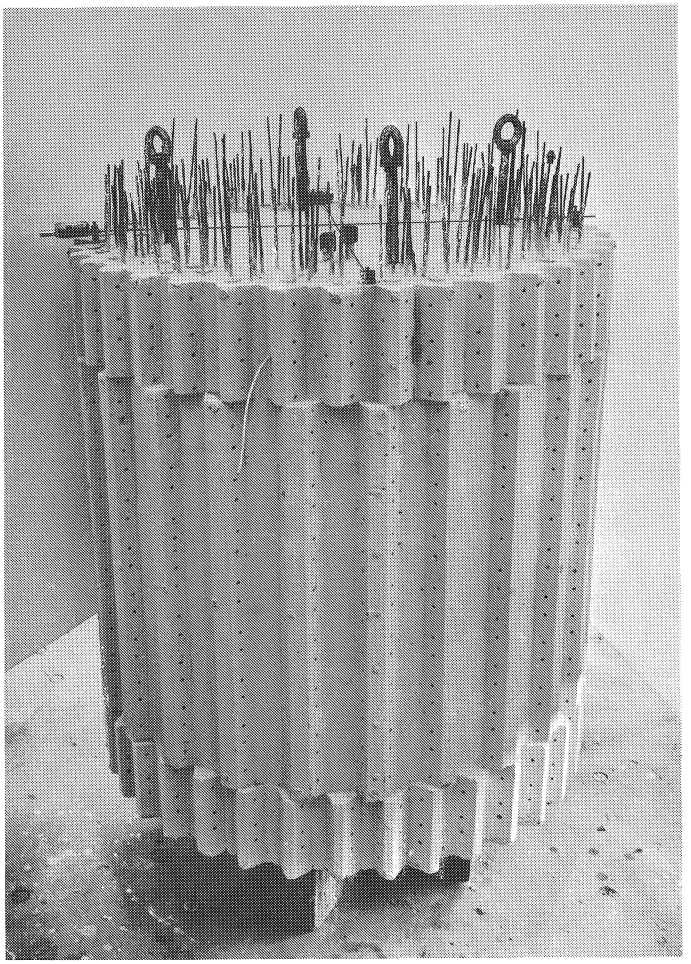

Fig. 17. Model pressure vessel after stripping of formwork and removal of forming wires for horizontal and vertical prestressing steel(including removal of plastic sheathing).

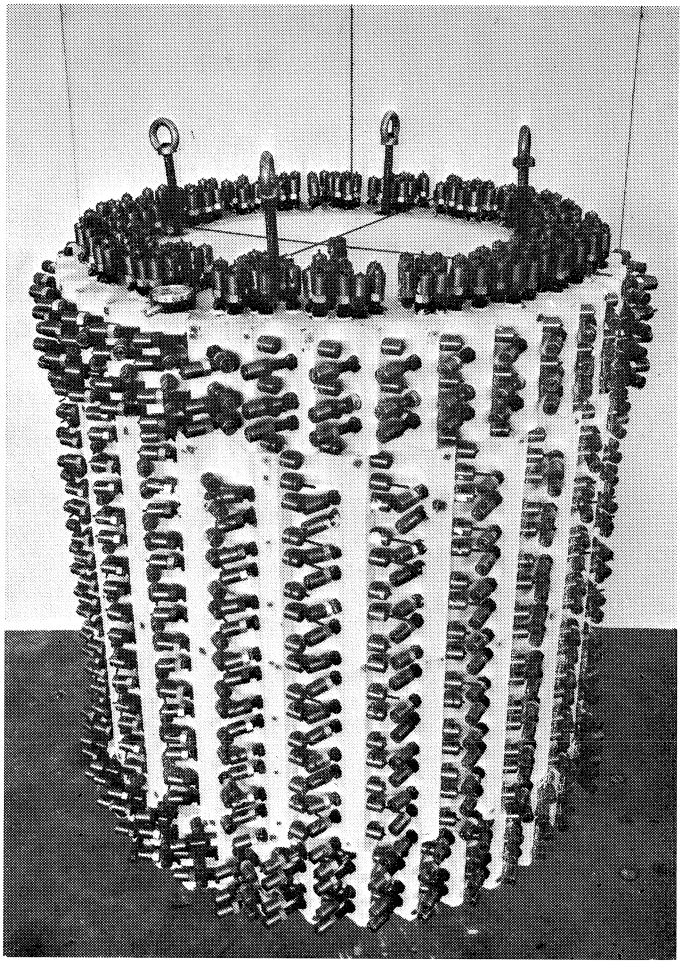

Fig. 18. Model pressure vessel after prestressing.

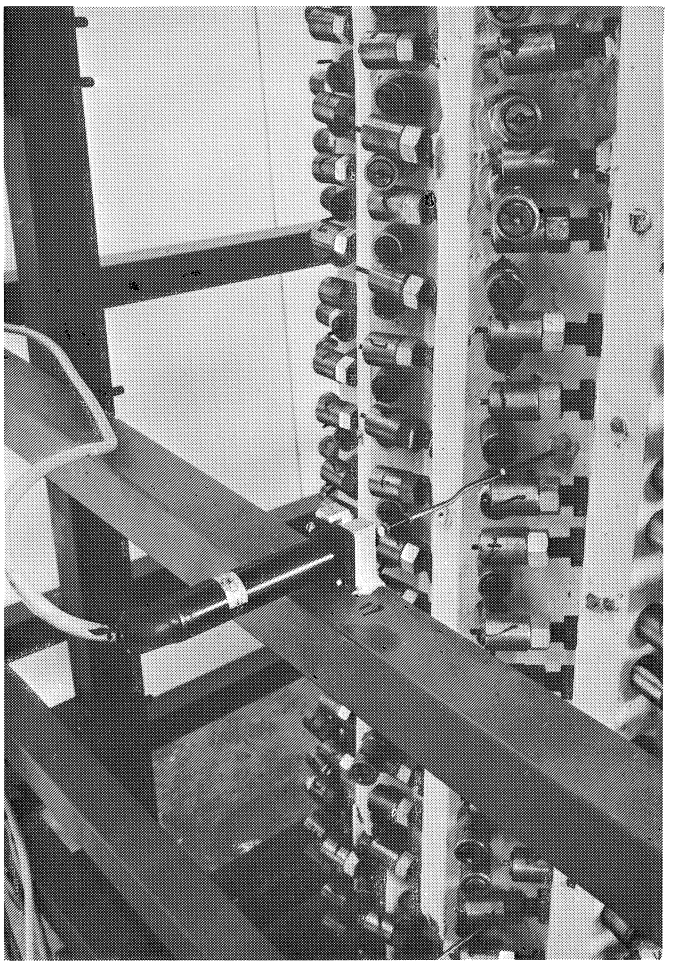

Fig. 19. Detail of deformation measuring apparatus: displacement transducers

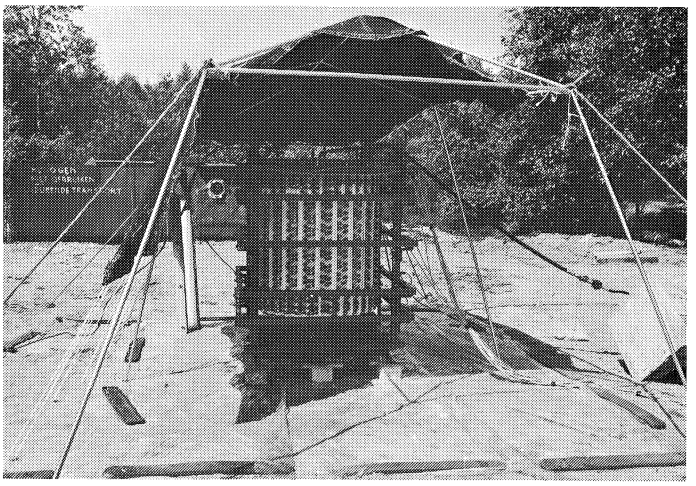

Fig. 20.
Model pressure vessel before being loaded by internal gas pressure

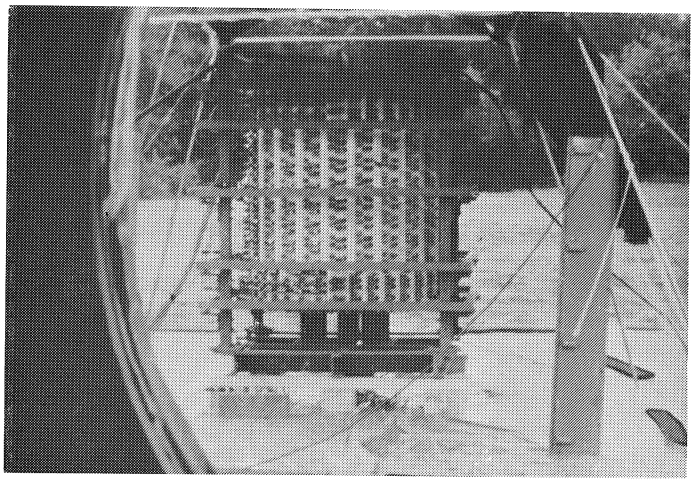

Fig. 21.
Last photograph of the model before failure

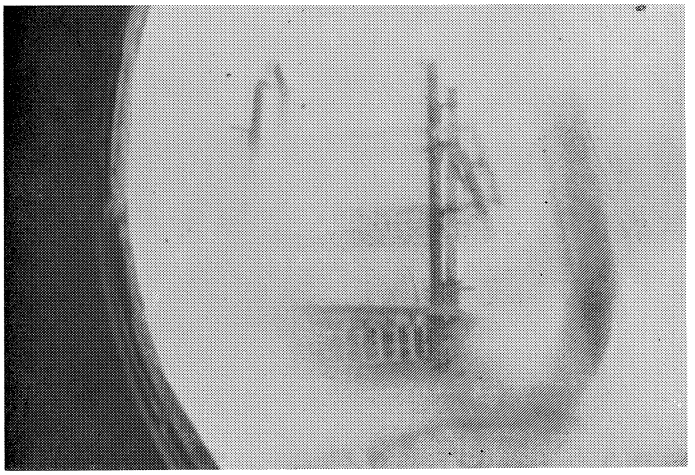

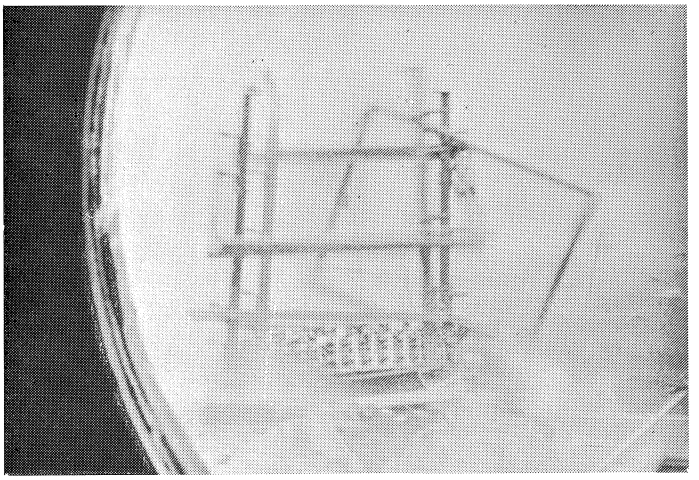

Fig. 21.
Photographs taken after failure of the model

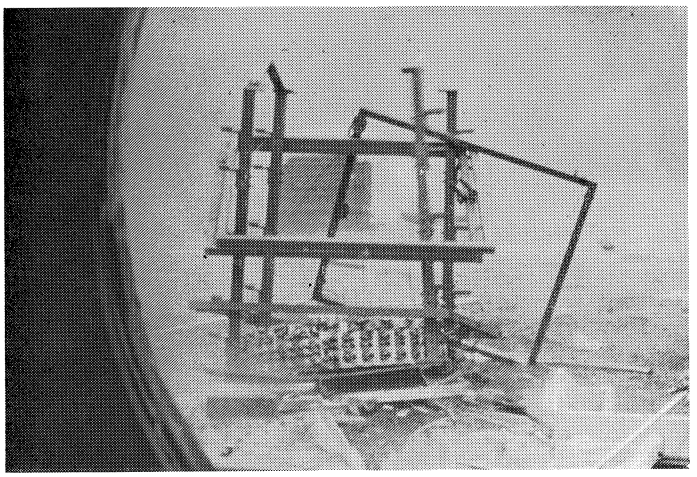

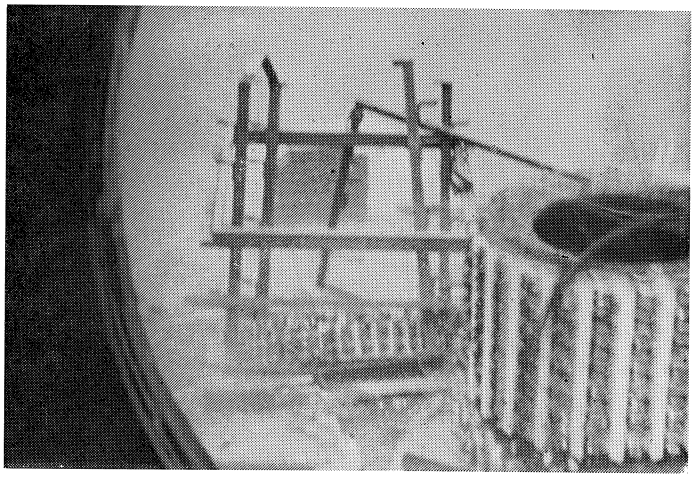

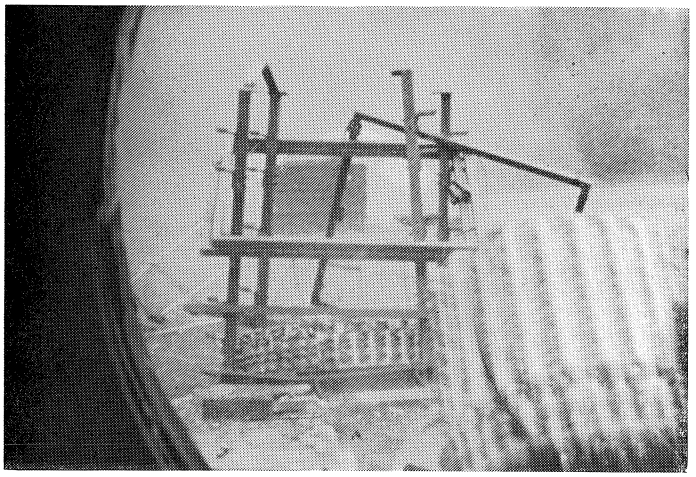

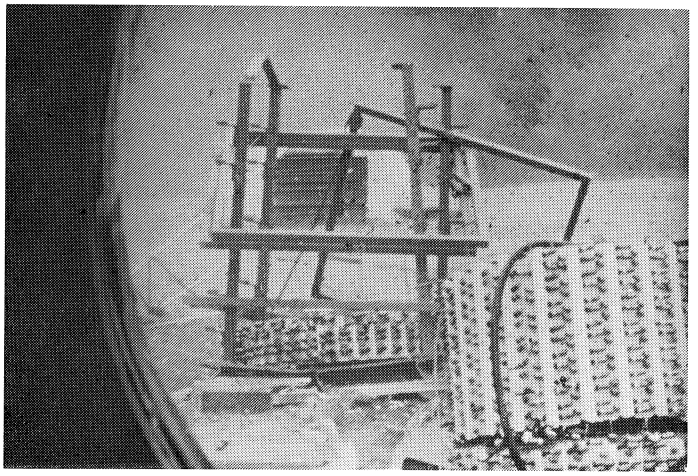

Fig. 22. General view of the model after failure.

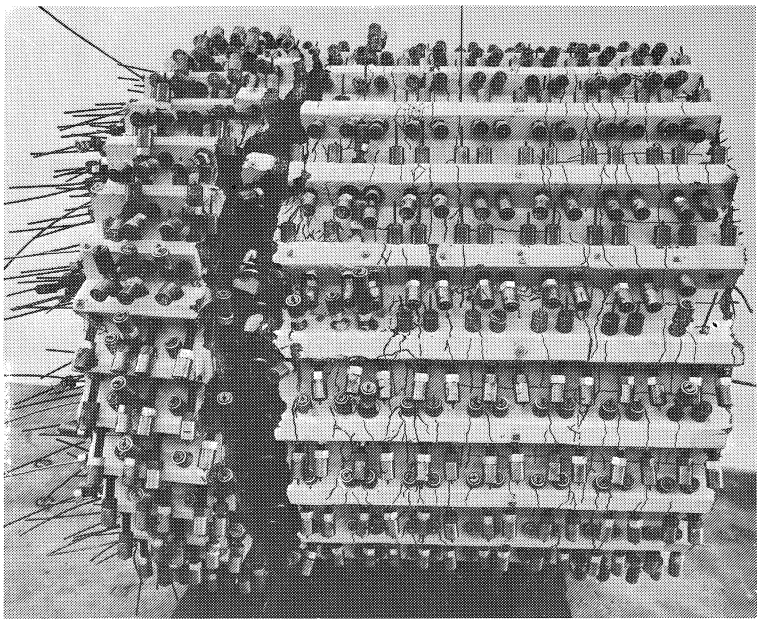

Fig. 23.
Cracking in the wall of the model.

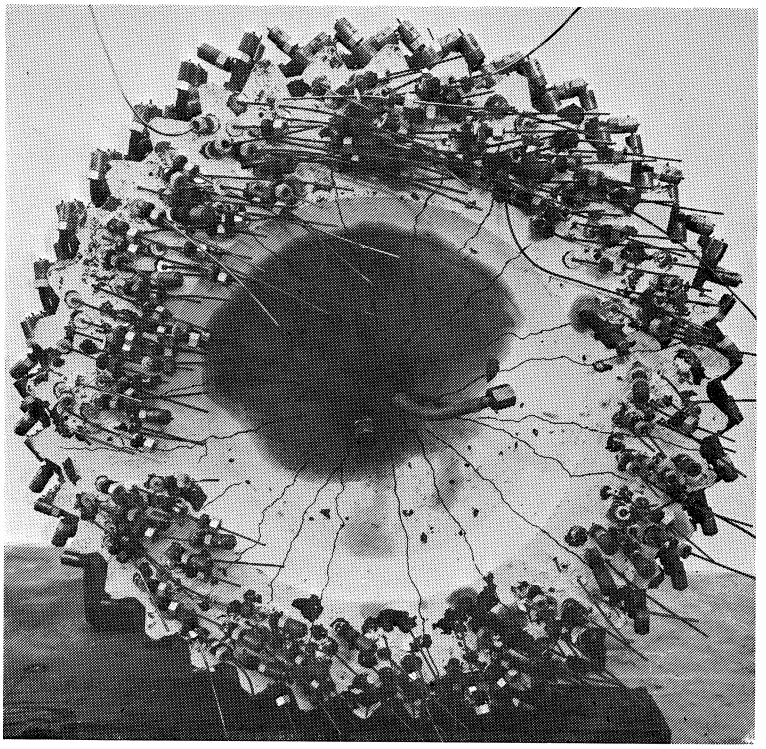

Fig. 24.
Cracking in the cover slab of the model.

13 Test-results

The deformations measured during loading with internal gas pressure are plotted against this pressure in Fig. 25. In that diagram the curve I relates to the change in cross-section of the vessel at mid-height, while curve II represents the average change in total height (average of four observations).

From this diagram it appears that up to about 7 MPa (70 kg/cm^2), i.e., 1.75 times the working pressure, the model remained uncracked and behaved in an elastic manner. Thereafter, with further increase in internal pressure, the deformations rapidly increased in consequence of cracking of the concrete. The factor of safety against cracking, referred to working pressure, was therefore 1.75. This figure does not allow for the temperature effect occurring under actual service conditions (see Section 4). For the wall of the vessel this factor is equal to the ratio of the permanent prestress to the stress due to working pressure, i.e., $9.54/5.54 = 1.75$, from which it appears that the tensile strength of the concrete was not able to make any contribution to the safety against cracking. This is not surprising, having regard to the shrinkage of the concrete (see Fig. 11) and the effect of temperature at the beginning of the hardening period (see Appendix 3), which together may well have caused cracking of the concrete before the prestress was applied.

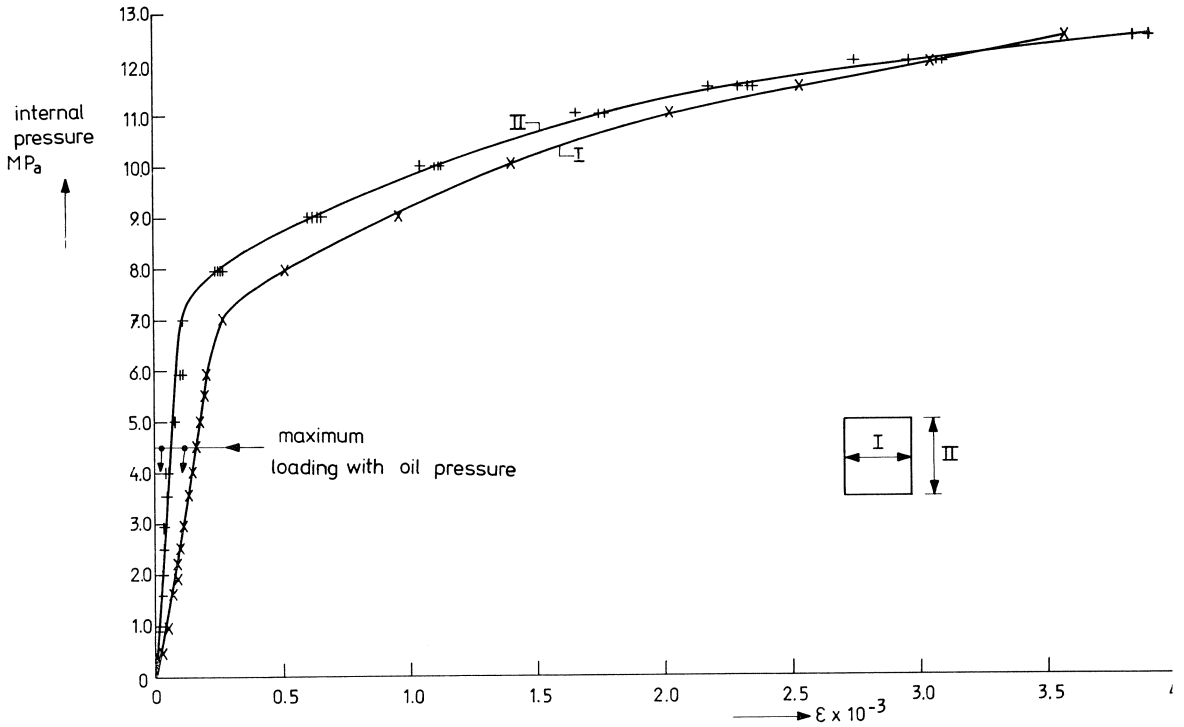

Fig. 25. Relation between internal pressure and mean specific deformation (strain) of the model pressure vessel.

The required margin between working load and failure (see Section 6), as represented by $\gamma = 3$, was amply attained in the test, since $12.9/4.0 = 3.2$. This is because the tensile strength of the prestressing steel (see Fig. 7) was 1720 MPa (172 kg/mm^2) instead of the nominal value of 1600 MPa (160 kg/mm^2) adopted in the design calculations. As a result the margin in relation to failure is theoretically increased to $\gamma = (1.72/1.60) \cdot 3 = 3.2$, which is in agreement with the measured value.

What exactly was the direct cause of the explosive failure that occurred is difficult to determine. However, there were two important aspects associated with this. First, a favourable factor, namely, the presence of 80 brass tubes in the failed section. These tubes theoretically make a substantial contribution to the strength of the structure and thus to the value of γ (in all, these tubes had a cross-sectional brass area of 298.4 mm^2, with a strength of 483 MPa and an elongation of 10% at failure). On the other hand, the second point is highly unfavourable: when the liner fractures, the area on which the pressure of 12.9 MPa (129 kg/cm^2) acts undergoes a considerable increase. In such a case the steel and the brass in the concrete would together have to develop a maximum force which is $88{,}8^2/56.8^2 \approx 2.5$ times the failure force for the non-fractured liner. Hence it appears very probable that the direct cause of

explosive failure of the vessel was fracturing of the liner, immediately followed by fracturing of the prestressing steel and brass tubes.

Despite the explosive character of the failure, it cannot be regarded as "sudden failure" in the ordinary sense of the term, since there was considerable increase in deformation after cracking and before failure occurred, as is evident from Fig. 25. In the case of a pressure vessel in actual practice there would thus be sufficient opportunity to adopt counter-measures in time and so prevent an explosion. Besides, it should be noted that overloading by a factor of 3 is not possible in reality. Actually, the pressure in the vessel cannot rise above a maximum equal to about 1.2 times the working pressure (in this case 4.8 MPa). But if this coincides with local damage to the liner and concrete – in which context a deterioration of the quality of the steel cannot be ruled out, since the temperature of the primary coolant is 650°C – a situation could arise that would demand prompt action. The increase in the total force in consequence of the increase in surface area when the liner fractures will then reduce the apparently available safety margin by an amount which may be quite substantial, depending on how serious the damage is.

14 Conclusion

From the research carried out it can be inferred that the safety of prestressed concrete pressure vessels deserves closer attention. The view that the hazard of explosive failure of such vessels is negligible is shown to be incorrect by this research, which was undertaken more particularly in order to test the validity of that view. A knowledge of the phenomena that occur provides an opportunity of taking adequate measures in the design of the pressure vessel.

References

1. Taylor, R. S., The Wylfa vessels. Conference on prestressed concrete pressure vessels, Paper 2. Westminster, London, S.W. 1, 13-17 March 1967.
2. Warner, P. C., The Dungeness B vessels. Conference on prestressed concrete pressure vessels, Paper 3. Westminster, London, S.W. 1., 13-17 March 1967.
3. Scotto, F., An improved system of hooping cables. Conference on prestressed concrete pressure vessels, Paper 3. Westminster, London, S.W. 1, 13-17 March 1967.
4. Eberle, K. and F. Schmiedel, Modellversuche am Spannbetonbehälter für einen 300 MW Hochtemperatur-Reaktor (Model tests on the prestressed concrete pressure vessel for a 300 MW high-temperature reactor). Information meeting on work relating to prestressed concrete vessels and their isolation, Brussels, 7-8 November 1967.
5. Torielli, E. and F. Scotto, Prestressed concrete pressure vessel for nuclear reactors – experiments on small models. Information meeting on work relating to prestressed concrete vessels and their isolation, Brussels, 7-8 November 1967.

APPENDIX 1

A. Analysis of the stresses in the pressure vessel

Stresses due to working pressure: 4 MPa (40 kg/cm^2)

- Vertical stresses in the wall:

$$\sigma_v = \frac{4.0 \cdot (\pi \cdot 568^2/4)}{2\pi \cdot (568+888)/4 \cdot 160}$$

$$= 2.78 \text{ MPa } (27.8 \text{ kg/cm}^2)$$

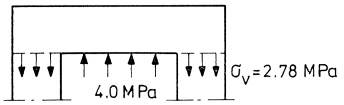

- Horizontal stresses in the wall, according to boiler formula:

$$\sigma_h = \frac{4.0 \cdot 568}{2 \cdot 160}$$

$$= 7.10 \text{ MPa } (71.0 \text{ kg/cm}^2)$$

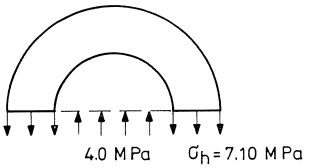

The model under consideration has relatively thick walls. The value calculated above is the average stress. The stress distribution through the thickness of the wall is given by:

$$\sigma_{hd} = 4.0 \cdot \frac{568^2 + 888^2}{888^2 - 568^2}$$

From this equation we obtain at the external surface (substituting $d = 568$): $\sigma_{hd} = 5.54$ MPa (55.4 kg/cm^2) and at the internal surface (substituting $d = 888$): $\sigma_{hd} = 9.55$ MPa (95.5 kg/cm^2).

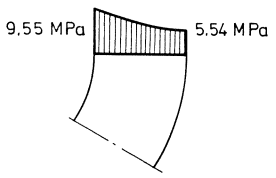

The internal pressure acting in the vessel is presumed to produce a bursting force, associated with a fictitious shearing plane at 60°, in the end slabs. The average stress acting in the circumferential direction as a result of this bursting force is:

$$\sigma_{hs} = \frac{4.0 \cdot (\pi \cdot 568^2/4) \cdot 568}{\pi \cdot 568 \cdot 182 \cdot 2 \cdot 160} \cdot \sqrt{3}$$

$$= 9.74 \text{ MPa } (97.4 \text{ kg/cm}^2)$$

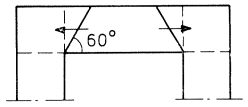

The stress $\sigma_{hs} = 9.74$ corresponds to an internal pressure on the end slabs equal to: $(9.74/7.10) \cdot 4.0 = 5.50$ MPa (55.0 kg/cm^2), i.e., approximately 1.4 times the working pressure.

If the effect of the thickness of the wall is taken into account, the stresses in the end slabs are as follows:
at the external surface: $(5.50/4.0) \cdot 5.54 = 7.62$ MPa (76.2 kg/cm^2), at the internal surface: $(5.50/4.0) \cdot 9.55 = 14.40$ MPa (144.0 kg/cm^2).

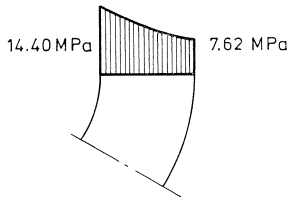

Shear force must also be taken into account in the end slabs. This force is calculated from the pressure acting in the vessel. The maximum shear stress under working load conditions is:

$$\tau = \frac{4 \cdot (\pi \cdot 568^2/4)}{\pi \cdot 568 \cdot 182} = 3.16 \text{ MPa } (31.6 \text{ kg/cm}^2),$$

so that the following values are obtained for the principal stresses in the end slabs:

$$\beta_{1,2} = \frac{5.50}{2} \pm \sqrt{\left(\frac{5.50}{2}\right)^2 + 3.16^2} = 2.25 \pm 4.19 \text{ MPa};$$

$$\beta_1 = -1.94 \text{ MPa } (19.4 \text{ kg/cm}^2) \text{ (tension)}$$

$$\beta_2 = +6.44 \text{ MPa } (64.4 \text{ kg/cm}^2) \text{ (compression)}$$

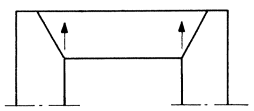

Stresses due to a temperature gradient:

$\Delta T = 20\,^{\circ}\mathrm{C}$

$\alpha_t = 1 \cdot 10^{-5}/^{\circ}\mathrm{C}$; $v = 0.15$

$E_b' = 40$ GPa (400000 kg/cm^2)

The horizontal stresses in the wall can be calculated by means of the equation:

$$\sigma_{ht} = -\frac{\mathrm{m}}{2(m-1)} \cdot E_b' \cdot \alpha_t \cdot \Delta T \cdot \left\{ \frac{1 + \frac{1}{\left(\frac{d}{568}\right)^2}}{1 - \frac{1}{\left(\frac{888}{568}\right)^2}} - \frac{\ln \frac{d}{568} + 1}{\ln \frac{888}{568}} \right\},$$

where $\mathrm{m} = 1/v$

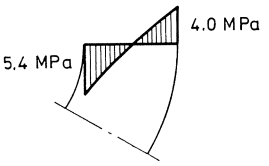

From this equation we obtain at the external surface, where $d = 888$:

$$\sigma_{ht} = +4.0 \text{ MPa } (40 \text{ kg/cm}^2)$$

and at the internal surface, where $d = 568$:

$$\sigma_{ht} = -5.4 \text{ MPa } (54 \text{ kg/cm}^2)$$

The vertical stresses at the external and the internal surface of the wall due to ΔT are equal to the respective horizontal stresses.

The horizontal stresses in the wall due to the working pressure of 4 MPa and the temperature gradient $\Delta T = 20\,^{\circ}\mathrm{C}$ are:

at the external surface: $\sigma_h = 5.54 + 4.0 = 9.54$ MPa (95.4 kg/cm^2)

at the internal surface: $\sigma_h = 9.55 - 5.4 = 4.15$ MPa (41.5 kg/cm^2).

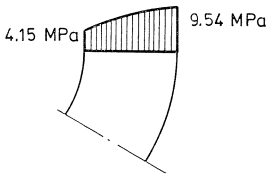

The vertical stresses in the wall due to the working pressure of 4 MPa and the temperature gradient $\Delta T = 20\,°C$ are:

at the external surface: $\sigma_v = 2.78 + 4.0 = 6.78$ MPa (67.8 kg/cm^2)

at the internal surface: $\sigma_v = 2.78 - 5.4 = -2.62$ MPa (-26.2 kg/cm^2).

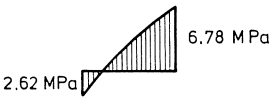

B. Calculation of the required quantity of reinforcing steel in bottom slab and cover slab to resist the shear force

The maximum shear stress in the cover slab and bottom slab under working load conditions (see Section A) is:

$$\tau = 3.16 \text{ MPa } (31.6 \text{ kg/cm}^2)$$

The quantity of prestressing steel was so determined that for $\gamma = 3$ – i.e., for 3 times the working pressure – this steel alone could still just resist the forces acting in the wall in the vertical and horizontal directions (see Section 6). Hence it follows that the shear force in these two end slabs must be resisted by additional steel: reinforcing steel. Since the two slabs must likewise have a safety margin of $\gamma = 3$, the quantity of such reinforcement in them must be sufficient to ensure that the maximum tensile force which it can develop is equal to the tensile failure load of the total vertical prestressing steel: in other words, equal to the total compressive force on the end slabs under failure load conditions.

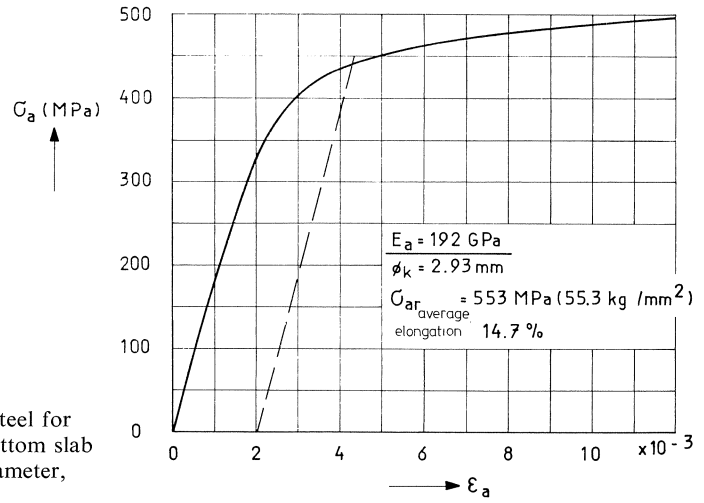

Fig. 1.1.
Stress-strain diagram of steel for reinforcement cages in bottom slab and cover slab: 3 mm diameter, grade QR 40.

On the basis of a failure mechanism at an angle of 45° the average tensile force per centimetre of circumference of the end slabs which the reinforcement is still just able to resist at failure of the vessel is:

$$3 \cdot 3.16 \cdot 182 \cdot 10 \cdot \sqrt{2} = 24100N = 24.1 \text{ kN } (2.41 \text{ t})$$

The following shear reinforcement was provided: 3 mm diameter wires, grade QR 40. The average stress-strain diagram for this type of wire is presented in Fig. 1.1.

Adopting the actual diameter and the actual tensile strength of the shear reinforcement employed, it must comprise at least:

$$\frac{24100}{\pi \cdot (2.93^2/4) \cdot 553} = 6 \text{ wires per lin. cm of circumference}$$

or 9 wires per 1.5 centimetres of circumference of the end slabs. The average horizontal centre-to-centre distance of the individual wires was 1.5 cm (see Figs. 5 and 9).

APPENDIX 2

Frictional losses associated with prestressing

Before the actual prestressing of the model was commenced, the frictional losses associated with the tensioning of the vertical and horizontal tendons were determined.

For the vertical tendons this friction measurement was performed on some of the wires installed in brass tubes. These wires were tensioned from one end only, the force applied being 10 kN (1 t), while the other end was of course securely anchored. Anchorage cones were used for anchoring the prestressing wires. After the wires had been tensioned and anchored, the forces acting at the two ends of each wire were measured. These measurements as well as the measurement of the prestressing force of 10 kN (1 t) were performed by means of load cells placed between the anchorage cones and the concrete wall. The cells were connected to a Peekel monitoring and control cabinet.

From the measured values the average coefficient of friction and the average force distribution along the straight wires were calculated by means of the equation:

$$P_a = P_A(1-\mu\beta a) = P_0(1+\mu\beta a) \tag{2.1}$$

where:

P_A = tensioning force applied to the end of the wire; in this case $P_A = 10$ kN (1 t);
P_0 = average prestressing force at end of wire after anchorage thereof and release of the tensioning device;
P_a = prestressing force at a section of the wire located at a distance "a" from the tensioning end;
a = distance from any particular section of a wire to the tensioning end;
β = random angular change per lin. cm;
μ = coefficient of friction.

The average coefficient of friction and the average distribution of force along the individual wires are indicated in Table 2.1, while the force distribution is furthermore presented schematically in Fig. 2.1. From the values stated in Table 2.1-a it follows that the loss of prestressing force due to friction of the vertical wires installed in brass tubes is 15% on average (for tensioning from one end only). This value served as a basis for determining the initial prestressing force P_A for the vertical prestressing wires, this being the tensioning force applied to the end of the wire so as to ensure that, after deduction of the frictional loss, the prestressing force remaining at any particular section of the wire will be at least equal to the value required there. A

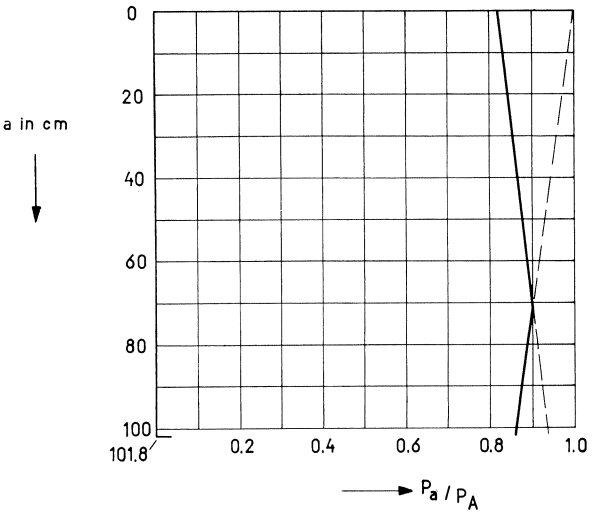

Fig. 2.1.
Distribution of force along vertical wires in brass tubes.

Table 2.1a. Calculation of average coefficient of friction for vertical prestressing wires in brass tubes.

wire No.	P_A (kN)	P_o (kN)	P_a*)(kN)	P_o/P_A	P_a/P_A*)	$1-P_a/P_A$*)	$\mu\beta$ (1/cm')
1	10	8.45	8.48	0.845	0.848	0.152	0.0015
2	9	8.39	8.61	0.932	0.957	0.043	0.0004
3	9	7.00	7.25	0.778	0.805	0.192	0.0019
4	9	6.65	7.07	0.739	0.785	0.215	0.0021
5	9	7.25	7.77	0.805	0.863	0.137	0.0013
average		7.55	7.84	0.820	0.852		0.0014

*) $a = 101.8$ cm.

Table 2.1b Calculation of distribution of prestressing force along vertical wires in brass tubes.

a (cm)	$\mu\beta_{av.} \cdot a$	$1-\mu\beta_{av.} \cdot a$	$1+\mu\beta_{av.} \cdot a$	$0.820(1+\mu\beta_{av.} \cdot a)$	
20	0.028	0.972	1.028	0.843	$P_a=P_o(1+\mu\beta a)$
40	0.056	0.944	1.056	0.866	$=0.820P_A(1+\mu\beta_{av.} \cdot a)$
60	0.084	0.916	1.084	0.889	
80	0.112	0.888	1.112	0.912	
100	0.140	0.860	0.140	0.935	
101.8	0.143	0.857	1.143	0.937	

value of 15% was adopted also for the frictional loss of prestress in those vertical prestressing wires which were not installed in brass tubes.

As a result of slip losses on anchorage the initial prestressing force P_A in fact undergoes a decrease at the very outset. This decrease is of about the same order of magnitude as the frictional loss: see Table 2.1 and Fig. 2.1. The maximum force in the vertical wires after anchorage is then still approximately 0.90 P_A (see Fig. 2.1).

For the horizontal prestressing steel the frictional loss was determined for one layer of tendons in the cover slab and one layer in the wall. The wires in these layers were first tensioned with a force of 10 kN (1 t) at one end and immediately thereafter at the other end, the wire of course being anchored at the non-tensioning end. The anchorage of these wires after tensioning, and the measurement of the forces at the ends of the wires, were carried out in the same manner as already described for the vertical prestressing wires.

The average coefficient of friction and the distribution of force along the individual curved wires were calculated by means of the equation:

$$P_\varphi = P_A \cdot e^{-\mu\varphi} = P_0 \cdot e^{\mu\varphi} \tag{2.2}$$

The frictional losses in the straight portions of the horizontal wires were neglected.

In equation (2.2):

P_φ = prestressing force at a section of the wire at which the wire has turned through a total angle φ in relation to the initial point;

φ = total angle through which the wire has turned at any particular section in relation to the initial point.

For the meaning of the symbols P_A, P_0 and μ see equation (2.1).

The average coefficient of friction and the average force distribution along the individual wires of the horizontal tendon layer in the cover slab and in the wall are indicated in Tables 2.2 and 2.3 respectively, while the force distribution is furthermore presented schematically in Figs. 2.2. and 2.3 (for the cable arrangement and magnitude of the angles see Figs. 2 and 3 respectively).

From Tables 2.2-a and 2.3-a it follows that for all the horizontal prestressing wires the loss of prestressing force due to friction – for tensioning the wires from both ends – can be taken to have the following average value:

$$\frac{\frac{1-0.399}{2} + \frac{1-0.288}{2}}{2} \cdot 100\% = 33\%$$

This value of the frictional loss of prestressing force was adopted as the basis for determining the initial prestressing force P_A for the horizontal tendons.

As in the vertical tendons, this initial force is decreased at the very outset as a result of losses due to slip on anchorage. The maximum force in the horizontal wires after anchorage is 0.84 P_A on average (see Figs. 2.2 and 2.3).

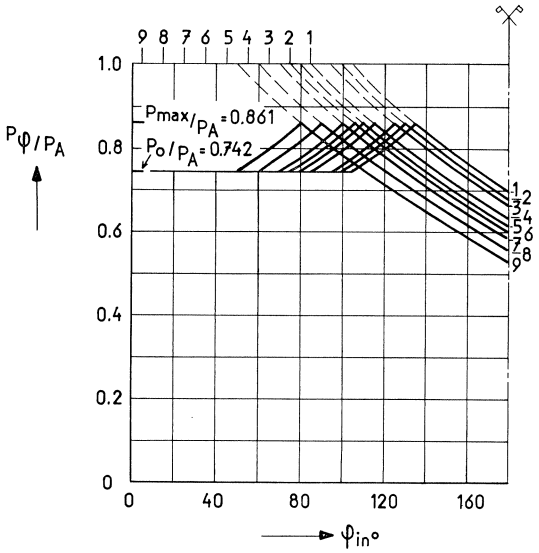

Fig. 2.2.
Distribution of force along individual wires for horizontal prestress in cover slab of model.

Table 2.2a Calculation of average coefficient of friction for prestressing wires in cover slab of model.

wire No.[1])	φ (in °)	φ (in rad.)	P_A (kN)	P_φ (kN)	P_φ/P_A	$\ln(P_\varphi/P_A)$	μ (1/rad.)
1	150	2.62	10	5.63	0.563	−0.574	0.219
2	160	2.79	10	5.48	0.548	−0.601	0.215
3	170	2.96	10	4.14	0.414	−0.882	0.298
4	190	3.31	10	3.11	0.311	−1.168	0.353
5	200	3.49	10	2.55	0.255	−1.367	0.392
6	210	3.66	10	5.19	0.519	−0.656	0.179
7	220	3.84	10	5.67	0.567	−0.567	0.148
8	240	4.19	10	2.98	0.298	−1.211	0.289
9	260	5.34	10	1.13	0.113	−2.180	0.408
avergae	200				0.399		0.278

[1]) wires numbered from outside to inside (see also fig. 2).

Table 2.2b Calculation of distribution of prestressing force along wires in cover slab model.

φ (in °)	φ (in rad.)	$\mu\cdot\varphi$	P_φ/P_A	
20	0.35	0.097	0.908	$P_A = 10$ kN (1 t)
40	0.70	0.195	0.822	$P_o = 742$ kg $\quad P_o/P_A = 0.742$
60	1.04	0.289	0.750	$\varphi_m = (1/2\mu)\cdot\ln(P_o/P_A) = 30.8°$
80	1.39	0.386	0.679	$P_{max} = \sqrt{P_A\cdot P_o} \rightarrow P_{max}/P_A = 0.861$
100	1.74	0.484	0.617	
120	2.09	0.581	0.560	
140	2.44	0.678	0.508	$P_\varphi = P_o\cdot e^{\mu\varphi}$
160	2.78	0.773	0.462	
180	3.14	0.873	0.418	$\varphi = 20° \rightarrow P_\varphi/P_o = 1.10 \rightarrow P_\varphi/P_A = 0.816$

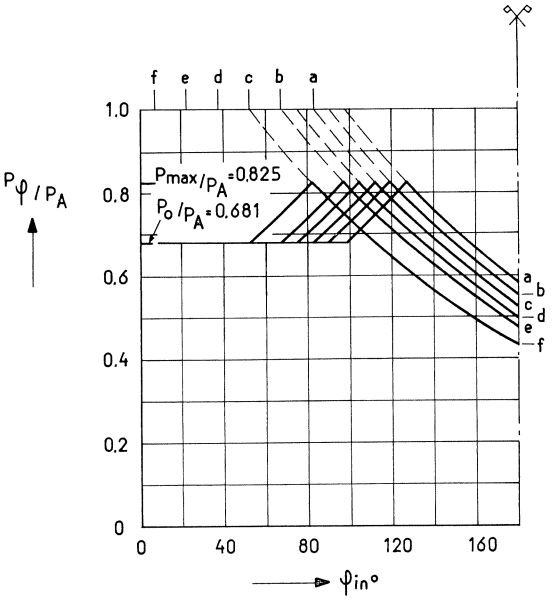

Fig. 2.3.
Distribution of force along individual wires for horizontal prestress in wall of model.

Table 2.3a Calculation of average coefficient of friction for prestressing wires in wall of model.

wire No. [1])	φ (in °)	φ (in rad.)	P_A (kN)	P_φ (kN)	P_φ/P_A	$\ln P_\varphi/P_A$	μ (1/rad.)
a	165	2.88	10	6.15	0.615	—0.486	0.169
b	180	3.14	10	3.56	0.356	−1.033	0.329
c	195	3.40	10	2.32	0.232	−1.461	0.430
d	210	3.66	10	1.90	0.190	−1.661	0.454
e	225	3.92	10	1.52	0.152	−1.884	0.481
f	255	4.45	10	1.83	0.183	−1.698	0.382
avergae	205				0.288		0.374

[1]) wires numbered from outside to inside (see also Fig. 3).

Table 2.3b Calculation of distribution of prestressing force along wires in wall of model.

φ (in °)	φ (in rad.)	$\mu\varphi$	P_φ/P_A	
				$P_A = 10$ kN (1 t)
20	0.35	0.131	0.878	
40	0.70	0.262	0.770	$P_o = 681$ kg $\quad P_o/P_A = 0.681$
60	1.04	0.389	0.678	
80	1.39	0.520	0.595	$\varphi_m = (1/2\mu)\cdot\ln(P_o/P_A) = 29.4°$
100	1.74	0.651	0.522	
120	2.09	0.782	0.458	$P_{\max} = \sqrt{P_A \cdot P_o} \rightarrow P_{\max}/P_A = 0.825$
140	2.44	0.913	0.402	$P_\varphi = P_o e^{\mu\varphi}$
160	2.78	1.040	0.354	
180	3.14	1.174	0.309	$\varphi = 20° \rightarrow P_\varphi/P_o = 1.14 \rightarrow P_\varphi/P_A = 0.776$

APPENDIX 3

Construction of the model

The procedure for constructing the model was as follows:

- The reinforcement was installed in the bottom slab formwork (Fig. 13) and other parts of the formwork.
- The 80 vertical brass tubes were assembled on the bottom panel of the formwork.
- The prefabricated forming rings for the horizontal tendons were placed around the 80 brass tubes. The individual forming wires were passed at their correct heights through openings provided for them in the wall of the formwork and were secured to the brass tubes (Fig. 14).
- Plastic-sheathed forming wires for the vertical tendons were slid upwards to their correct position through the perforated bottom panel of the formwork.
- The reinforcement cage for the bottom slab was installed after the forming rings for the horizontal tendons in the bottom slab had been fixed in position (Fig. 15).
- The procedure described above was continued, while the formwork was further assembled.
- Assembly was stopped on reaching a height corresponding to the top of the liner in the pressure vessel. After all the forming wires for the vertical tendons had been secured in correct position and height, the bottom slab of the pressure vessel was first concreted and then the liner was installed (Fig. 16). The liner served also as the internal formwork for the wall of the vessel, which was next concreted to a height of about 5 cm below the top of the liner (concreting stage I).
- The concrete surface for forming the construction joint was roughened by hacking and all the embedded horizontal forming wires (including their plastic sheathing) were removed. This was done one day after concreting stage I.
- Next, the final formwork ring, the remaining forming rings for the horizontal tendons, the reinforcement cage for the cover slab and the reinforcement at the top of this slab were installed in their correct sequence.

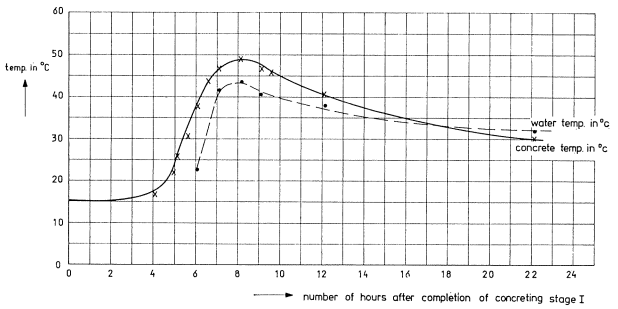

Fig. 3.1 Temperature curve for the micro-concrete used for the model.

- The forming wires for the vertical tendons were again secured and the rest of the pressure vessel was concreted (concreting stage II). There was an interval of 11 days between these two concreting operations. Both after stage I and after stage II the liner was filled with water which was kept at a temperature as close as possible to the measured temperature of the concrete during hardening. (The curve for the temperatures after concreting stage I is presented in Fig. 3.1). This was done in order to obviate the occurrence of stresses due to a temperature difference between the concrete and the interior of the vessel.
- The remaining horizontal and all the vertical forming wires (including their plastic sheathing) were removed. This was done one day after concreting stage II (Fig. 17).
- The prestressing tendons (wires) were installed and tensioned. These wires were inserted into the ducts formed in the concrete on removal of the forming wires and their plastic sheaths. The tendons were not grouted.

Fig. 18 shows the model pressure vessel after the wires had been tensioned.